Reconstruction of Electron Temperature Profiles Using Bayesian Analysis on Electron Cyclotron Emission Diagnostics in CHD

Fumiyoshi KIN[1)]*, Tatsuya KOBAYASHI[2)], Tokihiko TOKUZAWA[2)], Daiki NISHIMURA[2)], Takeo HOSHI[2)], Makoto SASAKI[3)], Kazunobu NAGASAKI[1)], Sigeru INAGAKI[1)]

[1)] *Institute of Advanced Energy, Kyoto University, Uji, Kyoto 611-0011, Japan*
[2)] *National Institute for Fusion Science, National Institutes of Natural Sciences, Toki, Gifu 509-5292, Japan*
[3)] *College of Industrial Technology, Nihon University, Narashino, Chiba 275-8575, Japan*

(Received 31 October 2025 / Accepted 27 January 2026)

The electron cyclotron emission (ECE) diagnostics is planned to be installed in the CHD stellarator/heliotrons for electron temperature measurement. The radiation profile of ECE is simulated by raytracing code, TRAVIS. Due to the insufficient optical thickness, the radiation temperature can be deviate from the electron temperature. To reconstruct the electron temperature profile, we have developed the analysis method based on the Bayesian framework, ODAT-SE. The method examined for several scenarios, including the wall reflections and energetic electrons. We have accurately reconstructed the electron temperature profile in all scenarios if the electron density profile is priorly given.

Keywords: electron cyclotron emission, CHD, TRAVIS, Bayesian analysis

DOI: 10.1585/pfr.21.1402023

1. Introduction

The electron cyclotron emission (ECE) diagnostic is a useful tool to measure electron temperature and is applied in many laboratory devices [1]. Although the ECE diagnostic is relatively easy to install, the interpretation of the data should be done carefully. If the optical thickness is not sufficient, the obtained radiation temperature does not reflect the local electron temperature. The energetic electrons can cause to make error in electron temperature measurement. The magnetic field structure is also important for determining the resonance location and its width. In particular, medium-sized stellarator/heliotrons are likely to encounter these problems [2]. Typically, ray tracing codes are used to interpret the data [3]. However, due to the lack of the quantitative estimates, different interpretations are occasionally possible, and the consistent electron temperature profile is not easily determined only from the ECE data. Therefore, the straightforward framework for reconstructing radiation temperature is demanded.

The ECE diagnostic is planned to be installed in CHD, which is the medium-sized heliotron device upgraded from CHS [4]. In this paper, an ECE systems in CHS is described, and the radiation temperature is simulated by raytracing code, TRAVIS [3]. Under the several scenarios, which includes wall reflections and energetic electrons, the radiation temperature can be deviated from the electron temperature. To deal with this problem, we have developed the reconstruction method using ODAT-SE [5], which is based on the Bayesian framework. The method is tested by synthetic data, and we obtain a reliable electron temperature profile from frequency-dependent radiation temperature, provided that the electron density profile is known in advance. We discuss the application of the method to real experimental data, as well as its potential extensions.

*Corresponding author's e-mail: kin.fumiyoshi.7m@kyoto-u.ac.jp

2. ECE Diagnostics in CHD

The CHD has the L/M = 2/8 helical coils and four poloidal coils. A maximum magnetic field strength at the magnetic axis B_{ax} reaches around 2 T, with a major and an averaged minor radii of 1 and 0.2 m, respectively. In this paper, we set B_{ax} = 1.4 T for study ECE diagnostics. As shown in Fig. 1, the ECE measurement will be provided at the horizontally elongated cross section, with the line of sight (LOS) located at the mid-plane. Unlike in tokamaks, the magnetic field profile in the CHD peaks near the plasma center, which can cause several EC resonances, as seen in Fig. 1. This is similar to LHD, where ECE measurements are provided from both the inboard and outboard sides to investigate the full radius of electron temperature profile [6]. In this paper, for the basic study, we investigate ECE measurement only from the outboard side.

Using TRAVIS, the details of the magnetic field components along the central ray trajectory are calculated, as shown in Fig. 2. The target of the electron temperature measurement is the 2nd harmonics X-mode radiation. In the case of B_{ax} = 1.4 T, the frequency range of 2nd harmonics EC within the last closed flux surface, $|\rho| \leq 1$, is approximately between 47

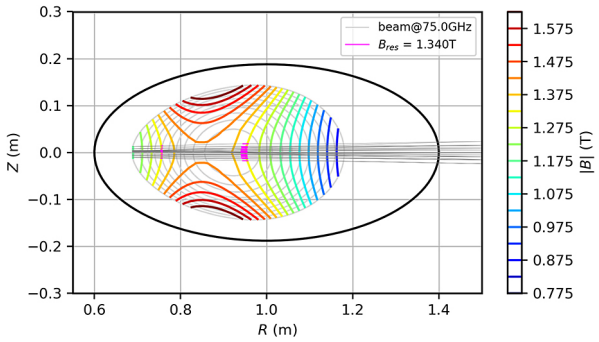

Fig. 1. Schematic view of raytracing of ECE at 75 GHz in CHD.

and 80 GHz, which can be seen in Fig. 1(a). Here, ρ indicates the normalized minor radius, and positive/negative ρ indicate inner/outer radii. The contamination from the emission at inner resonance can occur with the frequency more than 66 GHz. Figure 2(b) shows the magnetic field components of parallel (B_{para}), azimuthal (B_{azim}) and elevation (B_{elev}) angles to the ray. Since $B_{para} = 0$ is achieved in the entire radius, the LOS is perfectly perpendicular to the magnetic field lines. Therefore, the effect of the Doppler shifts can be neglected. The perpendicular magnetic field component is important for the polarization. As seen in Fig. 2(c), the angle between the elevation and the azimuth of the magnetic field lines varies with radius. Since the rotation of the polarization conserves the X-mode emission if only electron density is not extremely low [7], the polarization angles of all frequencies are determined at the outer edge ($\rho = -1$), which is about 61.5 degree. In this study, we neglect the mode conversion between the X-mode and the O-mode, and we carry out the analysis only on the X-mode.

3. Simulation of ECE and Electron Temperature in Several Scenarios

As explained in the introduction, due to the low optical depth and the complex magnetic field, radiation temperature observed in ECE cannot be simply proportional to the electron temperature profiles. From the radiative transport equation, a radiation temperature T_{rad} at frequency f is defined as, $T_{rad}(f) = \frac{2\pi c^2}{f^2} I_f$, where $I_f = I_f^{inc} e^{-\tau} + \frac{j}{\alpha}(1 - e^{-\tau})$ is the radiation intensity at the antenna assuming that $\frac{j}{\alpha}$ is uniform at the resonance. Here, j, α and τ indicate the emissivity, absorption coefficient, and optical depth, respectively. I_f^{inc} is the incoming radiation intensity at the start of the integration path. When $\tau \gg 1$, the radiation intensity corresponds to the blackbody radiation, $I_f \approx \frac{j}{\alpha} \approx \frac{f^2}{2\pi c^2} T_e$, and therefore, the radiation temperature reflects the electron temperature, $T_{rad}(f) \approx T_e$.

Using TRAVIS, we simulate the emission profiles of ECE and the expected radiation temperatures in several scenarios. As shown in Fig. 3, the electron temperature and electron density profiles are given for calculating ECE. Note that the peaked-T_e and hollowed-n_e profiles with a moderate central temperature ~ 1 keV and density ~ $1 \times 10^{19} m^{-3}$ are expected in CHD, which are the typical characteristics observed in the medium-sized stellarator/heliotrons [8]. To calculate ECE,

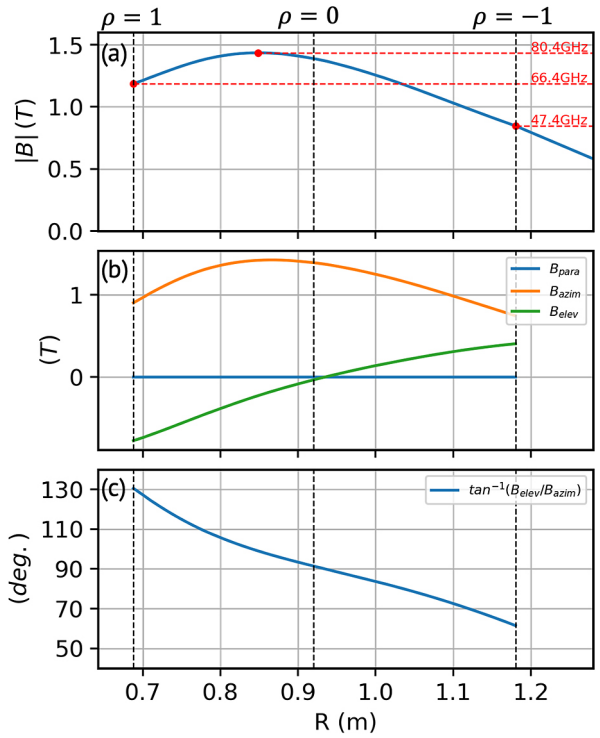

Fig. 2. Magnetic field profiles along the central ray trajectory for (a) intensity, (b) components, and (c) angle between elevation to azimuthal components.

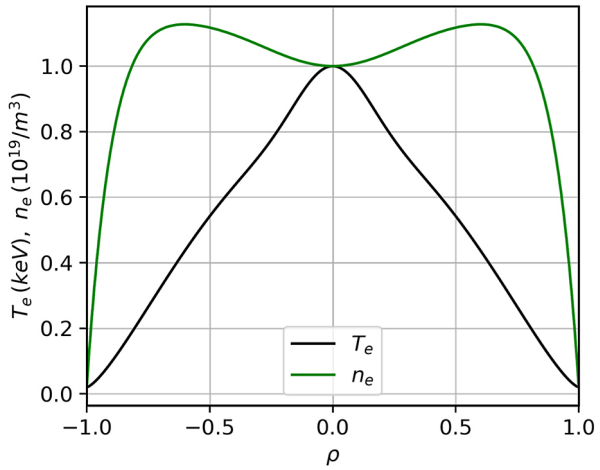

Fig. 3. Electron temperature and electron density profiles used to calculate TRAVIS.

effective charge number (Z_{eff}) is also given as 1 and uniform across the entire radial region. Here we mention that the input plasma profiles of $T_e(\rho)$, $n_e(\rho)$ and $Z_{eff}(\rho)$ are given by the fitting curves defined as, $\frac{f(\rho)}{f_0} = g - h + (1 - g + h)(1 - \rho^p)^q + h(1 - e^{-\rho^2/w^2})$, where f_0, g, h, p, q and w are 6 fitting parameters [3, 9].

Fixing the input plasma profiles as shown in Fig. 3, the emission profiles of ECE are simulated under three different conditions:

case 1: radiation from bulk electrons;

case 2: including wall reflection;

case 3: including energetic electrons via the bi-Maxwell

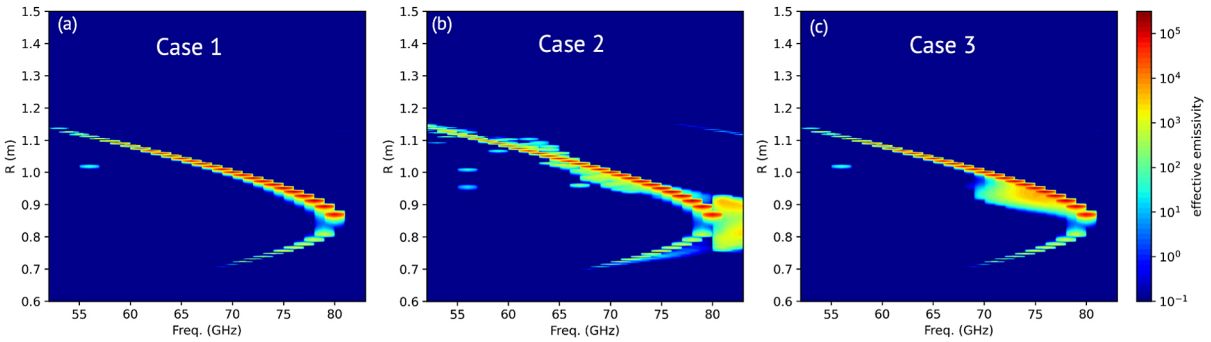

Fig. 4. Effective emissivity profiles of ECE with the conditions for (a) case 1, (b) case 2 and (c) case 3.

distribution.

The effective emissivity, which is the ECE emissivity taken into account the reabsorption, is shown in Fig. 4 for frequencies between 52 and 83 GHz. In case 1, the ECE is mainly emitted from the outward resonances. The emission from the inward resonance appears at f = 70–80 GHz, however, it's intensity is about 20 dB lower than that of the outward resonance. Therefore, the localization of ECE is almost satisfied. Note that the finite emission is appeared from f = 56 GHz at R ≈ 1.02 m, which is deviate from the resonance at the horizontally elongated flux surface. Due to the scattered reflections at the X-mode cutoff layer (which depend on the density profiles, with the scattered reflection occurring at f = 56 GHz in this case), the ray encounters the resonance at different toroidal locations, resulting in the observation of unexpected emission. This kind of unexpected emission can easily occur if the plasma is optically gray. The unexpected emission increases substantially when including the wall reflection, as shown in Fig. 4(b). Here, the reflection coefficient is taken as 1 for all the process, and the mode conversion due to the reflection is neglected for the calculation. Note that the finite emission is observed at frequencies above 80 GHz, where no ECE resonance exists at Fig. 2(a). The emission observed in this frequency range is completely unexpected, nonlocal emission derived by the wall reflection. Final scenario is case 3, considering the energetic electrons. In TRAVIS, the effect of energetic electrons is modeled via electron distribution function F_e as, $F_e = (1-\delta)F_{M0} + \delta F_{M1}$, where F_{M0} and F_{M1} are thermal and suprathermal components defined by Maxwellian distribution function [9]. Here, δ is a fraction of suprathermal component and is identical to the ratio of suprathermal to thermal electron density, $\delta = \frac{n_{e1}(\rho)}{n_{e0}(\rho)}$. Similarly, the suprathermal electron temperature is given by the ratio of suprathermal to thermal electron temperature, $\delta_T = \frac{T_{e1}(\rho)}{T_{e0}(\rho)}$. The radial dependence of these fractions is given as, $\delta(\rho) = \delta(0)e^{-\frac{\rho^2}{\Delta^2}}$ and $\delta_T(\rho) = 1 + \delta_T(0)e^{-\frac{\rho^2}{\Delta^2}}$. In this scenario, since we study suprathermal electrons generated by on-axis ECH injection, we calculate the emission profile using $\delta(0) = 0.05$, $\delta_T(0) = 4$ and $\Delta = 0.25$. The parameter $\Delta = 0.25$ indicates that the ECH deposition width should be smaller than 5 cm, and $\delta(0) = 0.05$ and $\delta_T(0) = 4$ correspond to a 20% energy fraction contained in suprathermal electrons at $\rho = 0$. These parameters are not strictly determined, but they are consistent with the estimates

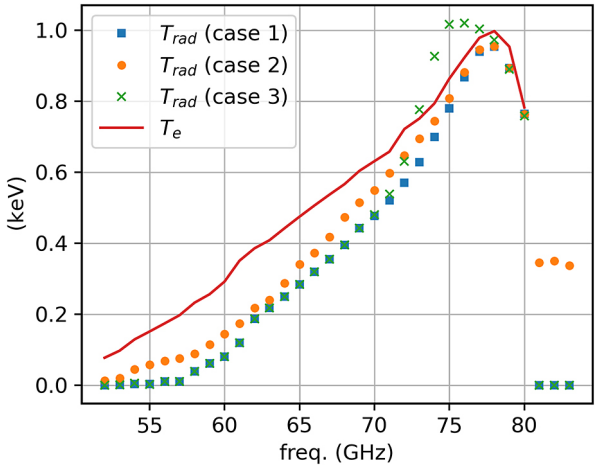

Fig. 5. Frequency-dependent radiation temperatures of ECE calculated in case 1 to 3. Electron temperature at the cold resonance frequency is also shown.

of ECH-driven suprathermal electrons discussed in Ref. [10]. As shown in Fig. 4(c), due to the relativistic mass increases, the frequency downshifted emission is induced from the central region ($f \sim 78$ GHz).

The radiation temperatures for all cases are shown in Fig. 5. In case 1, compared to the given electron temperature, the radiation temperature is small below $f \sim 75$ GHz. This is mainly due to the small optical thickness, which is about 2.5 at f = 75 GHz and about 1 at f = 70 GHz. In case 2, wall reflections somewhat increase the radiation temperature, however, it remains below compared to the electron temperature. To reduce computational cost, the number of reflections in the simulation is limited up to three, which might result in an underestimation of the radiation temperature. In case 3, due to the downshifted emission, radiation temperature at $f \sim 75$ GHz is increased. All of the scenarios indicate that the radiation temperature deviates from the expected electron temperature. Therefore, the reconstruction of the accurate electron temperature from ECE diagnostics is necessary, which will be addressed in the next section.

4. Reconstruction of Electron Temperature Profiles Using ODAT-SE

Reconstruction of the electron temperature profile from the observed radiation temperature is a typical inverse problem, which can be solved by searching the minimum value of the objective function G as, $G(X) = d(D_{cal}(X), D)$. Here, $X = (X_1, X_2, ..., X_n)$ is the target physical quantity from the observed data $D = (D_m, D_m, ..., D_m)$, and $D_{cal}(X)$ is a forward model that can represent D from X. A function $d(D_{cal}(X), D)$ denotes the distance between $D_{cal}(X)$ and D, which is frequently given as 2-norm.

The ODAT-SE provides several analysis algorithms to solve the inverse problem [5]. In this study, we applied Replica-exchange Monte Carlo method (REMC) for the analysis. Here we briefly introduce the method, and further details can be found in [5]. The objective is to obtain optimal value of X by minimize $G(X)$ from experimental data D. Using Bayes theorem, the conditional probability distribution of X under D can be written as, $P(X|D) = \frac{P(D|X)P(X)}{P(D)}$, where $P(D|X)$ is the likelihood function, $P(X)$ is the prior probability distribution of X, and $P(D) = \int P(D|X)P(X)dX$ is the normalized factor. Introducing the parameter τ called as 'temperature', the likelihood function can be represented as, $P(D|X) = \exp(-G(X;D)/\tau)$. The REMC method is performed by parallel calculations through Markov chain MC (MCMC) method on K independent systems (replicas) with different temperature $\tau_0, \tau_1, ...\tau_{K-1}$. During the calculation, the temperature is attempted to be changed between replicas, which is the advantage of this method to prevent the replicas from local minima. After the calculation, gathering all of the replicas, a temperature dependent distribution $P(X|D;\tau_i)$ can be obtained.

The schematic of the forward model is shown in Fig. 6. Note that the model depends on the scenarios. In the cases 1, 2 and 3, the target physical quantities X are the fitting coefficients of the electron temperature, which is introduced in Sec. 3. The solver of the forward problem $D_{cal}(X)$ is constituted by TRAVIS and the basic giving conditions, which are the magnetic surface information calculated by VMEC, the LOS (horizontally elongated cross section, mid-plane, outboard side) and beam width (~ 2.5 cm at focal point) of the optical system, the received center frequency (52–83 GHz) and their bandwidth (1 GHz), and profiles of $Z_{eff}(\rho) = 1$. Here, we assume that the electron density profile, $n_e(\rho)$, is a known parameter and is priorly given by the fitting coefficients. In the case 1, the forward model is constituted by these conditions. In the case 2, the wall reflection is added on the calculation of TRAVIS. In the case 3, the bi-Maxwell parameters of $\delta(0)$ and $\delta_T(0)$ are included in the target quantities.

Because the CHD is under the construction, the synthetic data is used as the experimental data D. The synthetic data of radiation temperature is prepared by TRAVIS calculated with the known electron temperature profile. Here, the synthetic radiation temperature is calculated by T_e and n_e profiles shown in Fig. 3. The calculated frequency-dependent radiation temperatures, which are identical to those shown in Fig. 5, are used as the experimental data D for the corresponding scenarios. In other words, we will predict the electron temperature profile that is shown in Fig. 3 from the synthetic data of radiation temperature shown in Fig. 5.

The calculation is performed through the REMC method with 20 replicas. Although using 20 replicas increases the computational cost, we selected this number to ensure sufficient overlap of calculations across temperatures. The computational cost mainly depends on the TRAVIS execution time for each step: approximately 7.6 s for Cases 1 and 3 (without wall reflection) and approximately 76 s for Case 2 (with wall reflection). In all scenarios, the objective function which should be minimized is the residual sum of squares (RSS) between the radiation temperatures evaluated by the forward model and the experimental values, as $F = \sqrt{\sum_f [T_{rad}(f) - T_{rad}^{exp}(f)]^2}$. After the calculations, the reconstructed electron temperature profiles are obtained from the fitting coefficients of the best results, which minimize the objective functions.

The results of cases 1, 2 and 3 are shown in Fig. 7. For all cases, the reconstructed (predicted) electron temperature profiles closely match the true electron temperature profiles except at the edge region. The discrepancy in the edge might be due to the small value of the optical thickness and the

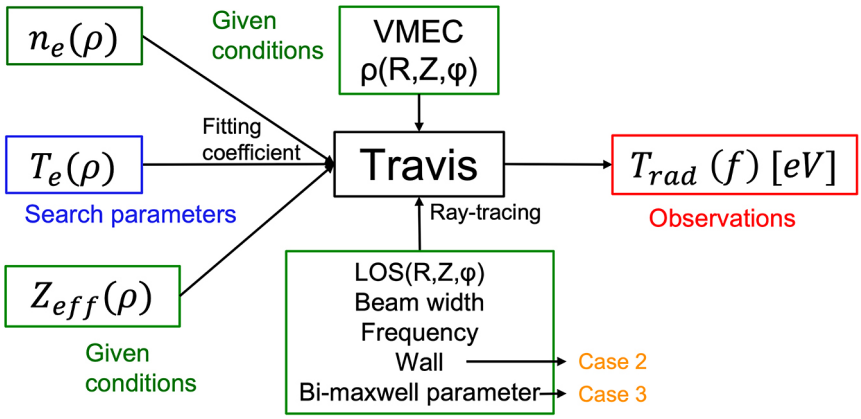

Fig. 6. Schematic view of forward model constituting the reconstruction method.

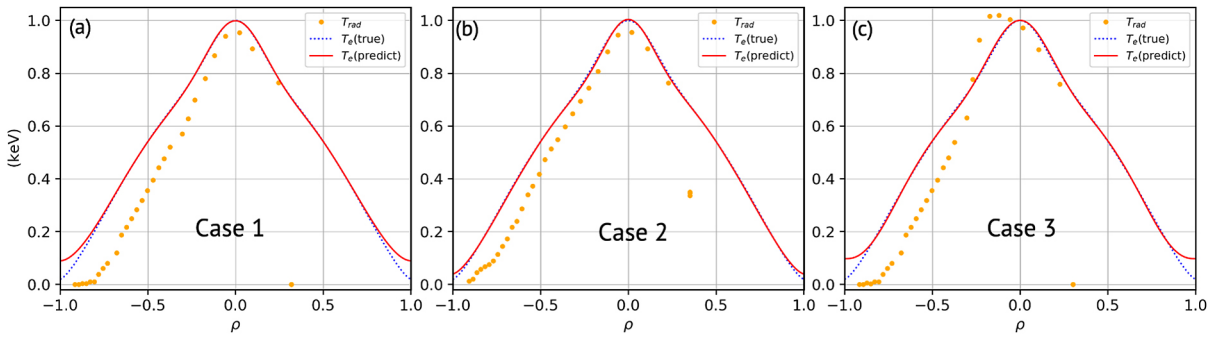

Fig. 7. The results of reconstructed (predicted) electron temperature profiles for (a) case 1, (b) case 2 and (c) case 3.

radiation temperature, which can increase the calculation error. The RSS between the true profiles and the predicted profiles are 0.071, 0.067 and 0.069 for cases 1, 2 and 3, respectively. Compared to the experimental data (input for the ODAT-SE), the analysis effectively reconstructs the electron temperature profile.

5. Discussion and Summary

The analysis method is beneficial for reconstructing the electron temperature profile from the ECE radiation profile. The method is expected to be applicable to real experimental data, however, we need to consider several points. First, the ECE data should include noise, which is mainly due to the thermal noise [11]. Since the thermal noise can be interpreted as a white Gaussian noise, we can include it in the framework. The effect of noise level on the analysis [12] should be clarified in the future. Next, we need to consider the mode conversion of ECE, which was neglected in this study. Particularly, the mode conversion can be important when the wall reflections significantly affect the ECE absorption. Installing the beam damp material [13] is one of the ways to reduce the reflection and simplify the interpretation of data. Finally, the absolute calibration of ECE diagnostics, which usually requires a lot of effort [14], is necessary for the analysis.

Although the analysis is a trial, the results suggest several potential applications using this framework. The interesting direction is to estimate the velocity distribution function of electrons. In case 3, which includes the bi-Maxwell parameters, the predicted parameters of $\delta(0) = 0.08$ and $\delta_T(0) = 3.3$ do not significantly deviate from true values, $\delta(0) = 0.05$ and $\delta_T(0) = 4$. Note that the bi-Maxwell parameters are not included in the objective function. If the electron temperature profile is known in advance, it is highly expected that these parameters can be predicted from the ECE data. Since the given electron distribution function in TRAVIS is limited, we need to develop the forward model that is suitable to study the energetic electrons [15]. The other direction is to develop a combination of the ECE and the multi-channel interferometer to reproduce T_e and n_e profiles. This can be beneficial for reactor measurements, where installing Thomson scattering diagnostics is difficult [16].

In summary, we have developed the reconstruction method of electron temperature profiles from the radiation profile of ECE. Using TRAVIS, the synthetic radiation temperatures in CHD are simulated in several situations, including the wall reflections and energetic electrons. The reconstruction method is formulated as an inverse problem based on the Bayesian framework, which can be effectively solved using ODAT-SE. The analysis provides improved reconstruction profiles in all of sinarios, if the electron density profile is given in advance.

Acknowledgements

The authors appreciate to CHD teams for their supports. This work is partly supported by the Grant-in-Aid for Scientific Research of JSPS, Japan (23K13084) and the collaboration programs of NIFS (NIFS23KUHL114 and NIFS10KUHL030).

[1] M. Bornatici *et al.*, Nucl. Fusion **23**, 1153 (1983).
[2] M. Luo *et al.*, Plasma Fusion Res. **15**, 2402038 (2020).
[3] N.B. Marushchenko *et al.*, Comput. Phys. Commun. **185**, 165 (2014).
[4] S. Okamura *et al.*, Nucl. Fusion **45**, 863 (2005).
[5] Y. Motoyama *et al.*, Comput. Phys. Commun. **280**, 108465 (2022).
[6] Y. Nagayama *et al.*, Fusion Eng. Des. **53**, 201 (2001).
[7] C. de Vries *et al.*, Phys. Plasmas **7**, 3707 (2000).
[8] F. Kin *et al.*, Phys. Plasmas **30**, 112505 (2023).
[9] N.B. Marushchenko *et al.*, Fusion Sci. Tech. **50**, 395 (2006).
[10] S. Coda *et al.*, Plasma Phys. Control. Fusion **48**, B359 (2006).
[11] C. Watts, Fusion Sci. Tech. **52**, 176 (2007).
[12] T. Kobayashi *et al.*, submitted to Rev. Sci. Instrum.
[13] T. Tokuzawa *et al.*, Rev. Sci. Instrum. **95**, 083531 (2024).
[14] U. Hefel *et al.*, Rev. Sci. Instrum. **90**, 043502 (2019).
[15] K. Yanagihara and S. Kubo, Plasma Phys. Control. Fusion **66**, 035002 (2024).
[16] Y.T. Lin *et al.*, Plasma Fusion Res. **17**, 1405098 (2022).